Published in final edited form as:
Wound Repair Regen. 2010 ; 18(1): 89–97. doi:10.1111/j.1524-475X.2009.00550.x.

Alteration in cellular morphology, density and distribution in rat vocal fold mucosa following injury

Changying Ling, Ph.D., **Masaru Yamashita, M.D., Ph.D.**, **Emily A. Waselchuk**, **Jennifer L. Raasch**, **Diane M. Bless, Ph.D.**, and **Nathan V. Welham, Ph.D.**
Department of Surgery, Division of Otolaryngology, University of Wisconsin School of Medicine and Public Health

Abstract

The vocal fold mucosa plays an important role in voice production. Its cellular composition and density frequently change under various pathological conditions, often contributing to altered extracellular matrix production, tissue viscoelasticity, and voice quality. In this study, cellular changes in the rat mucosa following a unilateral stripping injury were investigated and analyzed semi-quantitatively. Distinctive and sequential changes in cellular morphology, composition, and density were observed in the mucosa post-injury. Cellular recruitment was a major event during the early stage of injury and reached its peak level by day 5 post-injury. Several types of cells, including neutrophil-like cells, epithelial cells and fibroblast-like cells, were sequentially recruited. The sequential emergence of reactive cell populations following injury and subsequent reconstruction of the mucosa suggests their involvement in vocal fold tissue repair and scar formation processes.

Keywords

tissue repair; fibroblast; epithelial cells; histological changes; cellular reconstruction; stereological analysis

INTRODUCTION

The vocal fold mucosa is a layered structure comprised of epithelium and lamina propria (LP); both of which are superficial to the thyroarytenoid (TA) muscle. Together, these mucosal structures facilitate vocal fold immune, transport and barrier function, and underpin self-sustained tissue oscillation for voice production (1,2). The LP is especially important for vocal fold oscillation as it contains an extracellular matrix (ECM) rich in proteins and glycans with favorable viscoelasticity (3,4). The vocal fold mucosa is exposed to nearly continuous biomechanical impact stress during phonation with no negative consequence; however, significant tissue injury secondary to trauma, surgical resection, radiation, and various infectious and inflammatory processes can lead to disordered ECM remodeling, scar formation, and a profound dysphonia (5–7).

Alterations in cell composition and density in the vocal fold mucosa following tissue injury may contribute to the pathophysiology of scar formation; however, such cellular changes have received little attention in the vocal fold wound healing literature. The cellular make-up of the native human LP has been described based on histological analysis (8–10) and LP

Corresponding author: Nathan V. Welham, Ph.D., Department of Surgery, Division of Otolaryngology, University of Wisconsin School of Medicine and Public Health, K4/723 CSC, 600 Highland Avenue, Madison, WI 53792, Tel: +1-608-263-0121, Fax: +1-608-252-0939, welham@surgery.wisc.edu.

cell density has been estimated based on cell counting (8) and by measuring the ratio of DNA/protein content in digested tissue samples (11). These studies have provided useful data addressing the relative abundance, density and distribution of cells that inhabit the native LP (primarily fibroblasts, followed by myofibroblasts and macrophages); however, with the exception of one study addressing cell proliferation post-injury (12), little attention has been given to changes in mucosal cellularity under pathological conditions. Additionally, as the majority of work in this area has focused predominantly on the LP, there are limited data available describing the cellular characteristics of the vocal fold epithelium, particularly following tissue injury. Greater understanding of the events that follow vocal fold mucosal injury requires attention to resident and migrating cell populations in both the LP and epithelium. Moreover, improved knowledge of cellular changes is fundamental to eventual therapeutic manipulation of the vocal fold wound healing process.

We previously established a rat model for studying vocal fold mucosal injury and scar formation (12–14). The rat vocal fold has a mucosal architecture and LP ECM comparable to humans (15,16) and demonstrates a similar and robust response to tissue injury at the morphological, biochemical and functional vibratory levels (12–14,17–20). Published work in the rat has focused on inflammatory cytokine signaling, ECM protein/glycan abundance and organization, and tissue vibratory performance (13,14,18–22). Comparatively, there are a paucity of data addressing cellular changes in the vocal fold mucosa following injury, even though these cells mediate the post-injury inflammatory response and are responsible for the synthesis and regulation of local ECM. To address this important knowledge gap, we performed anatomical characterization followed by histological and semi-quantitative stereological analyses of changes in cellular morphology, density and distribution in the rat vocal fold mucosa following a unilateral stripping injury.

MATERIALS AND METHODS

Animals

Twenty-four 4-month-old male Sprague-Dawley (SD) rats with a mean body weight of 290 g (±10 g) were used in this study. Two naïve rats were used to establish a vocal fold atlas, one naïve rat was used for histological analysis of the vocal fold LP, sixteen rats received a unilateral vocal fold stripping injury, and five naïve rats were reserved as age-matched uninjured controls. All rats were housed in a pathogen-free facility at the University of Wisconsin School of Medicine and Public Health. All protocols involved in these experiments were approved by the Institutional Animal Care and Use Committee of the University of Wisconsin-Madison.

Surgery and tissue preparation

Vocal fold injuries were created as previously reported (13). Rats underwent anesthesia induction using isoflurane inhalation (2–3% delivered at 0.8–1.5 L/min), followed by maintenance with an intraperitoneal (IP) injection of ketamine hydrochloride (90 mg/kg) and xylazine hydrochloride (9 mg/kg). Atropine sulfate (0.05 mg/kg) was also injected IP to reduce the secretion of saliva and sputum in the laryngeal lumen. Under deep anesthesia, the rats were placed on an operation platform in a near vertical position, and a 1-mm-diameter steel wire laryngoscope was inserted to facilitate vocal fold exposure. A 1.9-mm-diameter 25° rigid endoscope (Richard Wolf, Vernon Hill, IL) connected to an external light source and video monitor was used for surgical monitoring. The right vocal fold mucosa was stripped using a 25-gauge needle, and injury was confirmed immediately by exposure of the TA muscle (Fig. 1C). Mucosal damage was consistent across experimental animals, and all rats recovered from surgery.

Euthanasia and laryngeal harvest were performed at four time points (four rats per time point): 1 day, 3 days, 5 days and 7 days post-injury. Each time point also included one or two additional age-matched control rats. All animals were euthanized via CO_2 asphyxiation, and larynges were harvested. Laryngeal specimens were immediately embedded in optimum cutting temperature compound (OCT, Tissue-Tek, Sakura, Tokyo, Japan), frozen with acetone and dry ice, and stored at −80° C. The larynges were sectioned at an interval of 8 μm in the coronal plane using a cryostat (CM-3050 S, Leica, Wetzlar, Germany). One-hundred serial sections, encompassing the majority of the vocal fold mucosa, were prepared from each laryngeal specimen. Every fifth section was subjected to routine hematoxylin and eosin (H&E) staining.

For the vocal fold atlas, two rat larynges were harvested and embedded for frozen sectioning. Four-hundred serial sections (8 μm interval, coronal plane) were prepared from each laryngeal specimen, encompassing the anterior commissure (AC), a structure at the anterior pole of the LP (Fig. 2A, B), and the arytenoid cartilage (ACT), to which the posterior end of the LP attaches (Fig. 2J, K, L). Every tenth section was subjected to routine H&E staining.

For histological analysis of the LP, one rat larynx was harvested, fixed in 4% paraformaldeyhde, embedded in paraffin, and sectioned at an interval of 10 μm in the coronal plane. Serial sections containing the LP were subjected to routine H&E staining.

All H&E stained sections were examined and imaged using a microscope (E-600, Nikon, Melville, NY) equipped with a digital microscopy camera (DP-71, Olympus, Center Valley, PA). Sections intended for stereological analysis were further imaged as described below.

Stereological analysis

We performed stereological analysis of vocal fold mucosa in both control and post-injury conditions using Stereo Investigator (MicroBrightField, Williston, VT). Stereo Investigator is a microscope based stereological analysis system designed for unbiased sampling of cell populations and biological features of interest, area measurement, and volume estimation. Large anatomical areas are mapped across multiple fields of view via motorized control of the microscope stage, and data from multiple fields and across serial sections can be integrated in the x, y and z planes. In this study, we employed an analysis set-up comprised of a Zeiss Axioplan 2 microscope (Carl Zeiss, Thornwood, NY) equipped with a digital microscopy camera (Carl Zeiss), motorized stage (XYZ controller, Ludl, Hawthorne, NY), and computer running Stereo Investigator software for instrument control, image capture and image analysis.

For each animal, two adjacent coronal sections containing the mid-membranous vocal fold mucosa at the level of the laryngeal ala cartilage (LAlc) (Fig. 2G, H; Fig. 3B) were selected for stereological analysis. The mid-membranous mucosa was selected as it is an important tissue region for vocal fold oscillation and was in the center of the tissue injury site in all injured samples; the LAlc was selected as an anatomical landmark to ensure that all analyses were performed at a consistent anterior-posterior level in the coronal plane. For each section, a contour was drawn around the border of the LP and the entire vocal fold mucosa. An open circle was selected as a marker for each individual cell within the LP, and markers were attached to the contour to provide coordinates. Mucosal/LP two-dimensional (2-D) cross-sectional area and LP cell density were computed, and a geomorphic map comprised of the contour and cell makers was exported for illustration and comparison within or across injury and control conditions.

Additional stereological analysis was performed for the H&E stained serial sections reserved for creation of the vocal fold atlas. Using these data, the volume of each mucosa/LP was estimated by multiplying the sum of all 2-D cross-sectional areas from the complete set of H&E stained serial sections by the interval between stained sections (80 μm in this study [we stained and analyzed every 10^{th} serial section]). Three-dimensional (3-D) reconstruction was performed by aligning a complete set of serial contours (Fig. 4A, each contour represents every 20^{th} serial section) at an anatomically correct interval (160 μm between contours, Fig. 4B), colligating the contours into a single unit, smoothing the luminal surface of the unit, and placing a cellular density map (the first contour in Fig. 4A) at the anterior border of the unit. 3-D reconstruction was performed using Adobe Illustrator CS3 (Adobe Systems, San Jose, CA).

Statistical analysis

Changes in mucosal cross sectional area and LP cell density post-injury were analyzed using repeated measures ANOVA. Pairwise comparisons across time points were performed for statistically significant main effects using Fisher's protected least squares difference (LSD). Analyses were performed using SAS 9.1.3 (SAS Institute, Cary, NC). An α-level of 0.05 was employed for all comparisons; all *p*-values were two-sided. Data were graphed showing mean ± standard error.

Results

Gross anatomy of rat vocal fold mucosa

The rat vocal fold mucosa is comprised of LP and epithelium, both of which are superficial to the TA muscle. In H&E stained tissue sections, the LP was distinguished from the epithelium and TA muscle by its relatively pale appearance and key structural features (Fig. 3). In the coronal plane, the anterior LP originated from the anterior commissure (AC in Fig. 2A, B) and its posterior pole attached to the arytenoid cartilage (ATC in Fig. 2J, K, L). Three-dimensionally, it was observed as an elongated structure (Fig. 4C) along its anterior-posterior (A–P) axis, with a length of approximately 1.4 mm and volume of approximately 0.17 mm^3. The medial-lateral (M–L) depth of the LP varied between 300 and 500 μm along its entire A–P axis (Fig. 4A, C). In the intact rat LP, the primary cell population appeared morphologically consistent with fibroblast-like cells. These cells contained spindle/star-shaped somata and multiple long processes, and were preferentially oriented along the superior-inferior axis (Fig. 3A). They were sparsely and randomly distributed throughout the majority of the LP, and densely distributed in four macula flavae (MF) regions located near the anterior and posterior poles bilaterally (aMF in Fig. 2B, C; pMF in Fig. 2I).

The luminal surface of the LP was covered by an epithelium comprised of darkly stained multiple layers of cells (Fig. 2, 3). These cells had short processes and their somata were closely aggregated along the mucosal surface. The superior epithelium contained stratified squamous cells (SSC in Fig. 3B and enlarged in Fig 7A). This stratified squamous cell layer gradually transitioned into a ciliated pseudocolumnar formation (CPF in Fig. 3B and enlarged in Fig. 7F) as the epithelium approached the inferior vocal fold boundary.

Morphological changes in rat vocal fold mucosa following a unilateral stripping injury

Our investigation of changes in the vocal fold mucosa post-injury focused on the mid-membranous mucosa at the level of the LAlc (Fig. 2G, H; Fig. 3B). The injury damaged the majority of the mucosa, created an open wound, and left a small amount of residual LP adjacent to the exposed TA muscle (indicated by an arrowhead in Fig. 1C).

Following injury, the damaged mucosa underwent a significant change in size, cell density, composition, and morphology (Fig. 5G to J); whereas the contralateral uninjured mucosa was largely unaffected (Fig. 5A to E). One day post-injury, a narrow strip of residual LP was observed at the injury site (Fig. 5G), and LP cell density was higher compared to control (Fig. 6A, B). The majority of these newly recruited cells had segmented nuclei (indicated by arrowheads in Fig. 6B), suggesting that they were neutrophil-like cells. Three days post-injury, the damaged LP had expanded in size (Fig. 5H). LP cell density was again higher than control, but appeared lower than those at the 1 day time point (Fig. 6C). The newly enlarged LP was populated by cells and trunks of fibrin matrix (indicated by a white arrow in Fig. 6C). A small number of cells had a neutrophil-like morphology (indicated by an arrowhead in Fig. 6C), whereas the majority had oval-shaped nuclei (indicated by black arrows in Fig. 6C). Five days post-injury, LP area had further expanded (Fig. 5I), cell density had further increased (Fig. 6D), and almost no fibrin matrix was observed (Fig. 6D). The majority of cells at this time point had oval-shaped nuclei and demonstrated wide variation in soma size. These cells had an increased number of processes compared with 3 days post-injury, and were randomly oriented. Seven days post-injury, LP area (Fig. 5J) and cell density (Fig. 6E) were unchanged compared with 5 days post-injury. Cell soma size appeared more consistent across the LP, and the majority of cells presented with a spindle-shaped morphology (arrows in Fig. 6E), bearing resemblance to the fibroblast-like cells present in the intact LP (Fig. 6A).

In parallel to the cellular changes noted in the LP, we observed distinct changes in the epithelial cell layer following vocal fold mucosal injury. As noted above, the injury completely stripped the mucosa. By 1 day post-injury, re-epithelialization had begun and the damaged LP was partially covered by a loosely organized cell layer (indicated by arrows in Fig. 7B). These cells lined the luminal surface of the residual LP and appeared morphologically distinct from the stratified squamous cells present in uninjured control epithelium (Fig. 7A). The inferior aspect of the epithelium was not stripped during the injury procedure, however its ciliated pseudocolumnar structure was flattened 1 day post-injury (indicated by an arrow in Fig. 7G). Three days post-injury, the entire luminal surface of the regenerating LP was covered by epithelial cells (Fig. 5H). This newly formed epithelial cell layer had an irregular thickness and was comprised of large cells (indicated by arrows in Fig. 7C) on its superior surface. These cells were loosely connected and embedded in fibrin matrix (indicated by arrowheads in Fig. 7C). The epithelial cell layer demonstrated reduced thickness, increased cell density, and altered cell morphology as it transitioned towards the inferior vocal fold boundary (Fig. 5H, 7H). The re-epithelialized mucosal segment integrated seamlessly with adjacent epithelial cells in both superior and inferior directions. Five days post-injury, the epithelial cell layer was further thickened (Fig. 5I), cell density was further increased, and fibrin matrix was undetectable (Fig. 7D). Seven days post-injury, epithelial thickness appeared unchanged (Fig. 5J) and cell density appeared decreased (Fig. 7E) compared with the 5 day time point. Of note at 7 days post-injury, a number of cells in the superior epithelium (indicated by arrowheads in Fig. 7E) displayed morphological resemblance to the stratified squamous cell characteristics of the control condition (white arrow in Fig. 7A).

Quantitative stereological analysis of mucosal cross-sectional area and LP cell density

We performed stereological analysis to obtain quantitative vocal fold mucosal cross-sectional area and LP cell distribution/density data across post-injury time points. In this analysis, a measurement probe was superimposed over a live image at 400 × magnification, and constant focusing was employed to accurately trace the border of the mucosa and LP, and visualize each individual cell in the LP (based on the presence of a cell nucleus within the 8 μm-thick H&E stained section). Contours of the mucosa and LP were generated, and

each cell within the LP was labeled with a small open circle (Fig. 8A). This geomorphic mapping provided quantitative cross-sectional area and cell density data in the coronal plane (Fig. 8B). Mucosal cross-sectional area demonstrated no statistically significant difference among controls (naïve animals with no injury to either vocal fold) and the uninjured vocal fold (contralateral to the injured vocal fold) in all experimental animals, but a significant change in the injured vocal fold over time (Fig. 8B, 9A). Compared to controls and the uninjured vocal fold, a significant reduction in area was observed 1 day post-injury, consistent with complete mucosal stripping. This observation was followed by a significant expansion in area at the 3, 5 and 7 day post-injury time points. In parallel to these changes in mucosal cross-sectional area, LP cell density increased significantly 1 day post-injury (Fig. 9B); as reported above, many of these cells showed neutrophil-like morphology (Fig. 6B). Cell density then decreased 3 days post-injury (Fig. 9B), potentially due to the corresponding rapid increase in mucosal area at this time point (Fig. 9A), the presence of extensive fibrin matrix, and the possible replacement of neutrophil-like cells by fibroblast-like cells. Cell density increased further and reached its peak at 5 days post-injury (Fig. 9B).

DISCUSSION

We characterized the gross anatomy of the rat vocal fold mucosa, generated an anatomical atlas and performed 3-D volumetric reconstruction, and observed significant changes in cellular morphology, density and distribution following a unilateral stripping injury. These histological changes occurred in a sequential fashion and involved both the epithelium and LP. When interpreted alongside previously published work focused on inflammatory cytokine signaling and ECM remodeling (18–20,23), these data help illuminate the early phases of vocal fold wound healing and may provide direction for new therapeutic efforts.

Our results showed that the luminal surface of the intact rat vocal fold mucosa contains a 2–3 layer stratified covering of squamous epithelial cells near its superior border, which transitions into multiple folded layers of ciliated pseudocolumnar epithelial cells towards its inferior border. This transitional epithelial structure is similar to that reported in human (4) and certain animal (16) vocal fold mucosae. In addition, we demonstrated that these epithelial cells undergo a significant change in composition, morphology, and density following injury. Initially, our stripping procedure completely removed the vocal fold epithelium. By 1 day post-injury, newly recruited epithelial cells with oval-shaped somata and nuclei were loosely aligned over the open wound, and residual ciliated pseudocolumnar cells near the inferior border of the vocal fold mucosa had flattened. The mucosa was completely re-epithelialized by 3 days post-injury; this newly formed epithelium consisted of multiple layers of large cells. By seven days post-injury, the luminal surface of the thickened epithelium was partially covered by squamous cells. This sequential reconstruction and transformation of the epithelium post-injury implies that efforts to manipulate this process may require time-sensitive strategies. Further, the altered morphology of the newly recruited epithelial cells may correspond to altered function. Previous work in human vocal folds has suggested that squamous epithelial cells retain their metabolic function right until the time of desquamation, at which time they are released into the lumen and replaced by dividing and migrating basal cells (4). Although the function of these squamous epithelial cells is not fully understood, they appear to play a role in mucus adherence, water and ion transport (1,24–26). The complete desquamation of vocal fold epithelial cells during the first 5 days post-injury suggests initial dysfunction of the epithelial layer, and the subsequent partial replenishment of squamous-like cells on the luminal surface by day 7 post-injury may correspond to early functional recovery. These hypotheses require confirmation by further functional investigation.

The native human LP is primary populated by fibroblasts, but is known to contain small numbers of myofibroblasts and, in some cases, macrophages (8). Fibroblasts and myofibroblasts share mesenchymal features and have similar morphology: Both feature spindle/star-shaped cell somata and have multiple long processes. One day post-injury, we observed massive recruitment of neutrophil-like cells (characterized by the presence of segmented nuclei) within the residual LP, indicating an acute inflammatory response. By 3 days post-injury, these neutrophil-like cells largely disappeared, and cells with relatively large somata and nuclei emerged. This change in cell population may reflect a functional transition from initial inflammatory response to early tissue repair. Also during this period, the LP significantly expanded in size and trunks of fibrin matrix (indicated by white arrows in Fig. 6C) appeared, primarily in the subepithelial region. Fibrin disappeared by day 5 post-injury (Fig. 5H,6D), indicating that fibrinolysis occurred between days 3 and 5. Fibrin is a fibrous protein and plays a key role in initial inflammatory response and blood clotting, signal transduction and protein polymerization (27). It is produced in various injured tissues where it acts as a provisional ECM for wound repair, and contributes to scar formation (27,28). Fibrin stimulates macrophages to synthesize transforming growth factor-β (TGF-β), which in turn induces fibroblast-to-myofibroblast differentiation and increased collagen production (29). The efficiency of fibrin degradation has been linked to scar formation and manipulation of this process has been employed as a strategy to improve wound healing outcomes in other tissues (28,30). Our data provide a time frame during which treatments targeted at dissolving fibrin and/or modulating its activators/inhibitors might be explored to attenuate vocal fold scar formation.

In this study, mucosal cross-sectional area and LP cell density and distribution were examined semi-quantitatively using stereological techniques. We measured the 3-D volume of the mucosa and mapped each individual cell within the LP. With the exception of the MF, all cells in the uninjured control samples were sparsely distributed throughout the entire LP. Quantitative analysis confirmed our observation of massive cell recruitment immediately post-injury, and identified peak LP cell density at 5 days post-injury. These findings are similar to a previous report that demonstrated peak cell proliferation 3 days following vocal fold mucosal injury in rats (12). Although cell density was relatively lower at 3 days post-injury in our study, active cell proliferation at this time point may underlie the sharp increase in LP cell density observed between 3 and 5 days post-injury. Further work is required to determine the relative contribution of proliferating resident cells and migrating circulatory cells to the overall increase in cell density observed post-injury.

We examined cellular composition and morphology in this study using H&E stained tissue sections. H&E is a commonly used stain in medical diagnosis and shows well-defined cell somata, nuclei and some processes. It is suitable for distinguishing and counting individual cells, and conveys general information regarding cell shape and size. H&E staining provides limited information for identifying and distinguishing cell types, and therefore allows only inferential statements regarding cell function. Our findings concerning cellular composition following vocal fold mucosal injury are primarily based on H&E staining, and are therefore preliminary. For this reason, we use the labels neutrophil-*like* and fibroblast-*like* (rather than neutrophil and fibroblast) in this paper. More accurate cell identification requires confirmation using antibodies against cell specific markers of interest, in an immunocytochemical (ICC) assay. Previous work suggests that the majority of proliferating cells in the LP post-injury are positive for the mesenchymal marker vimentin (12). We are conducting additional ICC to characterize both resident and migrating cell populations that may play a role in the inflammatory and tissue remodeling processes postinjury; these data are forthcoming.

In this study, mucosal stripping, a well established model of vocal fold injury in the rat (12,13), was used. The rat vocal fold shares many anatomical, cellular and extracellular features with the human vocal fold (2,3,5,11,12,13,14,21,22,23); however, it remains a relatively simple structure and exists in a clearly different biomechanical environment than that of human phonation. The wound healing and remodeling process culminating in vocal fold scar formation appears to occur more quickly in rodents compared with larger mammals (6,13,21); therefore, the sequential cellular alterations identified in this study may occur over an extended time period in humans. Additionally, mucosal stripping is no longer a widely used technique in contemporary phonosurgery, and is generally believed to differ in terms of wound healing outcome when compared to the injury sustained during microflap based microdissection, for example (31). Despite these caveats, our data provide a fundamental understanding of cellular alteration following vocal fold injury, which is an important area of investigation that has been largely neglected to date.

In conclusion, the native rat vocal fold mucosa is an elongated membranous tissue structure, sparsely populated with fibroblast-like cells and covered by stratified squamous and pseudocolumnar epithelial cells. Vocal fold stripping results in severe mucosal damage and leads to dramatic changes in LP and epithelial cell composition, morphology and density during the tissue recovery process. Re-epithelialization and normalization of mucosal area/volume occurs within 3 days post-injury. This volume recovery is accompanied by the recruitment of neutrophil-like, cells, epithelial cells and fibroblast-like cells; corresponding to a significant increase in LP cell density. These sequential cellular alterations may closely link to functional alterations, and therefore be important agents in the undesirable tissue repair events that lead to vocal fold scar and its associated dysphonia.

Acknowledgments

This work was supported by grant R01 DC4428 from the NIDCD. We gratefully acknowledge assistance with histologic interpretation provided by David Yang, M.D., and assistance with statistical analysis provided by Glen Leverson, Ph.D.

References

1. Sivasankar M, Fisher KV. Vocal fold epithelial response to luminal osmotic perturbation. J Speech Lang Hear Res. 2007; 50(4):886–898. [PubMed: 17675594]
2. Thibeault SL, Rees L, Pazmany L, Birchall MA. At the crossroads: Mucosal immunology of the larynx. Mucosal Immunol. 2009; 2(2):122–128. [PubMed: 19129759]
3. Gray SD, Titze IR, Chan R, Hammond TH. Vocal fold proteoglycans and their influence on biomechanics. Laryngoscope. 1999; 109(6):845–854. [PubMed: 10369269]
4. Gray SD, Titze IR, Alipour F, Hammond TH. Biomechanical and histologic observations of vocal fold fibrous proteins. Ann Otol Rhinol Laryngol. 2000; 109(1):77–85. [PubMed: 10651418]
5. Benninger MS, Alessi D, Archer S, Bastian R, Ford C, Koufman J, Sataloff RT, Spiegel JR, Woo P. Vocal fold scarring: current concepts and management. Otolaryngol Head Neck Surg. 1996; 115(5): 474–482. [PubMed: 8903451]
6. Rousseau B, Hirano S, Scheidt TD, Welham NV, Thibeault SL, Chan RW, Bless DM. Characterization of vocal fold scarring in a canine model. Laryngoscope. 2003; 113(4):620–627. [PubMed: 12671417]
7. Hansen JK, Thibeault SL. Current understanding and review of the literature: Vocal fold scarring. J Voice. 2006; 20(1):110–120. [PubMed: 15964741]
8. Catten M, Gray SD, Hammond TH, Zhou R, Hammond E. Analysis of cellular location and concentration in vocal fold lamina propria. Otolaryngol Head Neck Surg. 1998; 118(5):663–667. [PubMed: 9591866]
9. Gray SD. Cellular physiology of the vocal fold. Otolaryngol Clin North Am. 2000; 33(4):679–697. [PubMed: 10918654]

10. Rosenberg TL, Schweinfurth JM. Cell density of the lamina propria of neonatal vocal folds. Ann Otol Rhinol Laryngol. 2009; 118(2):87–90. [PubMed: 19326757]
11. Munoz-Pinto D, Whittaker P, Hahn MS. Lamina propria cellularity and collagen composition: an integrated assessment of structure in humans. Ann Otol Rhinol Laryngol. 2009; 118(4):299–306. [PubMed: 19462852]
12. Tateya I, Tateya T, Lim X, Sohn JH, Bless DM. Cell production in injured vocal folds: a rat study. Ann Otol Rhinol Laryngol. 2006; 115(2):135–143. [PubMed: 16514797]
13. Tateya T, Tateya I, Sohn JH, Bless DM. Histologic characterization of rat vocal fold scarring. Ann Otol Rhinol Laryngol. 2005; 114(3):183–191. [PubMed: 15825566]
14. Welham NV, Montequin DW, Tateya I, Tateya T, Choi SH, Bless DM. A rat excised larynx model of vocal fold scar. J Speech Lang Hear Res. 2009; 52:1008–1020. [PubMed: 19641079]
15. Hirano M. Structure of the vocal fold in normal and disease states: Anatomical and physical studies. ASHA Rep. 1981; 11:11–30.
16. Kurita, S.; Nagata, K.; Hirano, M. A comparative study of the layer structure of the vocal fold. In: Bless, DM.; Abbs, JH., editors. Vocal Fold Physiology: Contemporary Research and Clinical Issues. San Diego: College-Hill Press; 1983. p. 3-21.
17. Tateya T, Tateya I, Bless DM. Collagen subtypes in human vocal folds. Ann Otol Rhinol Laryngol. 2006; 115(6):469–476. [PubMed: 16805380]
18. Lim X, Tateya I, Tateya T, Muñoz-Del-Río A, Bless DM. Immediate inflammatory response and scar formation in wounded vocal folds. Ann Otol Rhinol Laryngol. 2006; 115(12):921–929. [PubMed: 17214268]
19. Welham NV, Lim X, Tateya I, Bless DM. Inflammatory factor profiles one hour following vocal fold injury. Ann Otol Rhinol Laryngol. 2008; 117(2):145–152. [PubMed: 18357839]
20. Ohno T, Hirano S, Rousseau B. Gene expression of transforming growth factor-beta1 and hepatocyte growth factor during wound healing of injured rat vocal fold. Laryngoscope. 2009; 119(4):806–810. [PubMed: 19213039]
21. Tateya T, Tateya I, Sohn JH, Bless DM. Histological study of acute vocal fold injury in a rat model. Ann Otol Rhinol Laryngol. 2006; 115(4):285–292. [PubMed: 16676825]
22. Tateya T, Tateya I, Muñoz-Del-Río A, Bless DM. Postnatal development of rat vocal folds. Ann Otol Rhinol Laryngol. 2006; 115(3):215–224. [PubMed: 16572612]
23. Ohno T, Hirano S, Rousseau B. Extracellular matrix gene expression during wound healing of the injured rat vocal fold. Otolaryngol Head Neck Surg. 2009; 140(5):757–761. [PubMed: 19393425]
24. Fisher KV, Telser A, Phillips JE, Yeates DB. Regulation of vocal fold transepithelial water fluxes. J Appl Physiol. 2001; 91(3):1401–1411. [PubMed: 11509542]
25. Sivasankar M, Fisher KV. Vocal folds detect ionic perturbations on the luminal surface: an in vitro investigation. J Voice. 2008; 22(4):408–419. [PubMed: 17280815]
26. Leydon C, Sivasankar M, Falciglia DL, Fisher KV. Vocal fold surface hydration: A review. J Voice. 2009; 23:658–665. [PubMed: 19111440]
27. Janmey PA, Winer JP, Weisel JW. Fibrin gels and their clinical and bioengineering applications. J R Soc Interface. 2009; 6(30):1–10. [PubMed: 18801715]
28. Sachs BD, Baillie GS, McCall JR, Passino MA, Schachtrup C, Wallace DA, Dunlop AJ, MacKenzie KF, Klussmann E, Lynch MJ, Sikorski SL, Nuriel T, Tsigelny I, Zhang J, Houslay MD, Chao MV, Akassoglou K. p75 neurotrophin receptor regulates tissue fibrosis through inhibition of plasminogen activation via a PDE4/cAMP/PKA pathway. J Cell Biol. 2007; 177(6): 1119–1132. [PubMed: 17576803]
29. Vidal B, Serrano AL, Tjwa M, Suelves M, Ardite E, De Mori R, Baeza-Raja B, Martínez de Lagrán M, Lafuste P, Ruiz-Bonilla V, Jardí M, Gherardi R, Christov C, Dierssen M, Carmeliet P, Degen JL, Dewerchin M, Muñoz-Cánoves P. Fibrinogen drives dystrophic muscle fibrosis via a TGFbeta/alternative macrophage activation pathway. Genes Dev. 2008; 22(13):1747–1752. [PubMed: 18593877]
30. Kisseleva T, Brenner DA. Mechanisms of fibrogenesis. Exp Biol Med (Maywood). 2008; 233(2): 109–122. [PubMed: 18222966]
31. Ford CN. Advances and refinements in phonosurgery. Laryngoscope. 1999; 109(12):1891–1900. [PubMed: 10591344]

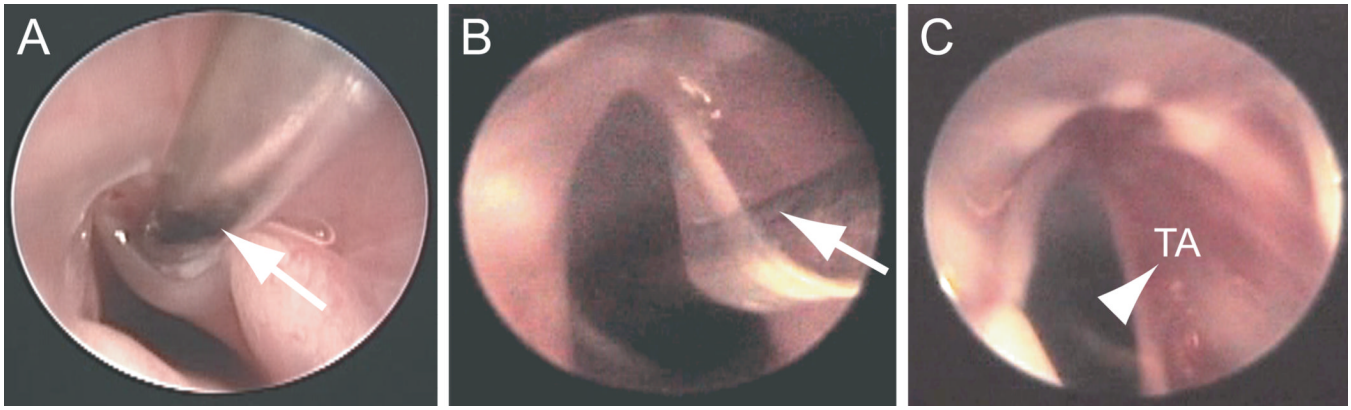

Figure 1.

Endoscopic images illustrating unilateral stripping of the right vocal fold mucosa in the rat. A: Needle insertion (indicated by an arrow) to the deep vocal fold mucosa. B: Rotation of the needle (indicated by an arrow) in the medial direction to separate the mucosa from the underlying thyroarytenoid (TA) muscle. C: Exposure of the TA muscle (indicated by an arrowhead) following injury.

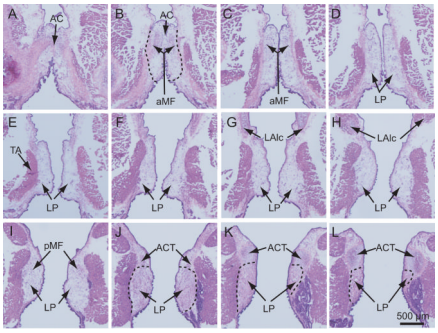

Figure 2.

Two-dimensional features of the rat vocal fold mucosa in the coronal plane along its anterior-posterior axis. The larynx was harvested from a naïve rat and processed for 8 μm frozen coronal sections. Every 10th section was subjected to routine H&E staining and imaged. Every other image containing the vocal fold mucosa (i.e., every 20th section; 160 μm between images) is presented in this figure from anterior (A) to posterior (L). The dashed line in B, J, K and L illustrates the boundary of the lamina propria.

AC: anterior commissure; ACT: arytenoid cartilage; aMF: anterior macula flava; LAlc: laryngeal ala cartilage; LP: lamina propria; pMF: posterior macula flava; TA: thyroarytenoid muscle.

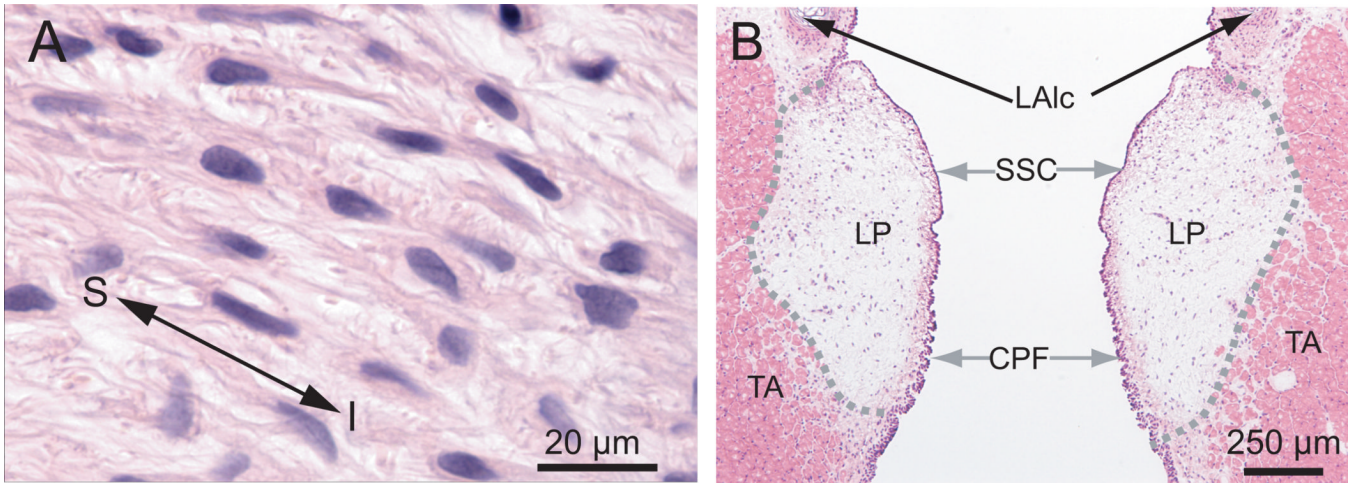

Figure 3.

Morphological characteristics of the naïve rat vocal fold mucosa in the coronal plane. A: An image of a paraffin section of the lamina propria (LP) illustrating fibroblast-like cells and their multiple long processes. B: An image of a frozen section of the rat vocal fold illustrating its gross anatomical structure.

CPF: ciliated pseudocolumnar formation; LAlc: laryngeal ala cartilage; LP: lamina propria; TA: thyroarytenoid muscle; SSC: stratified squamous cells. S: superior; I: inferior.

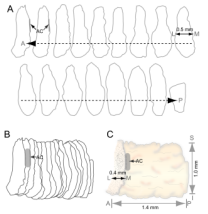

Figure 4.

Three-dimensional (3-D) reconstruction of the rat vocal fold mucosa. A: Serial two-dimensional contours of the mucosa in the coronal plane along its anterior-posterior axis. The interval between contours is 160 μm. B: Alignment and colligation of the serial contours. C: 3-D reconstruction of the mucosa based on the colligated contours. AC: anterior commissure; A: anterior; P: posterior; M: medial; L: lateral; S: superior; I: inferior.

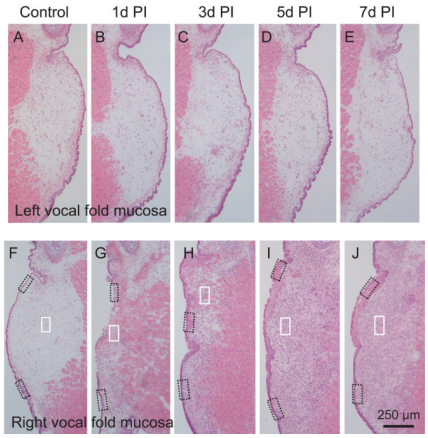

Figure 5.

Hematoxylin-eosin stained sections showing distinctive and sequential changes in gross anatomy following right-sided vocal fold mucosal injury in the rat. The left vocal fold mucosa represents an uninjured control tissue site within each experimental animal. Representative images from each experimental group show histological changes in both mucosal cross-sectional area and cellular density. Boxes in panels F–J are enlarged for better illustration and displayed in Figure 6 and Figure 7.

PI: post-injury.

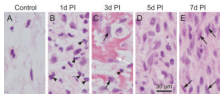

Figure 6.

Cellular changes in the rat vocal fold lamina propria following injury. Microscopy images (corresponding to small white boxes in Figure 5 F–J) at high magnification (400×) showing detailed cellular morphology. Arrowheads in B and C: neutrophil-like cells; Black arrows in C: newly recruited cells; White arrow in C: fibrin matrix; Arrows in E: fibroblast-like cells. PI: post-injury.

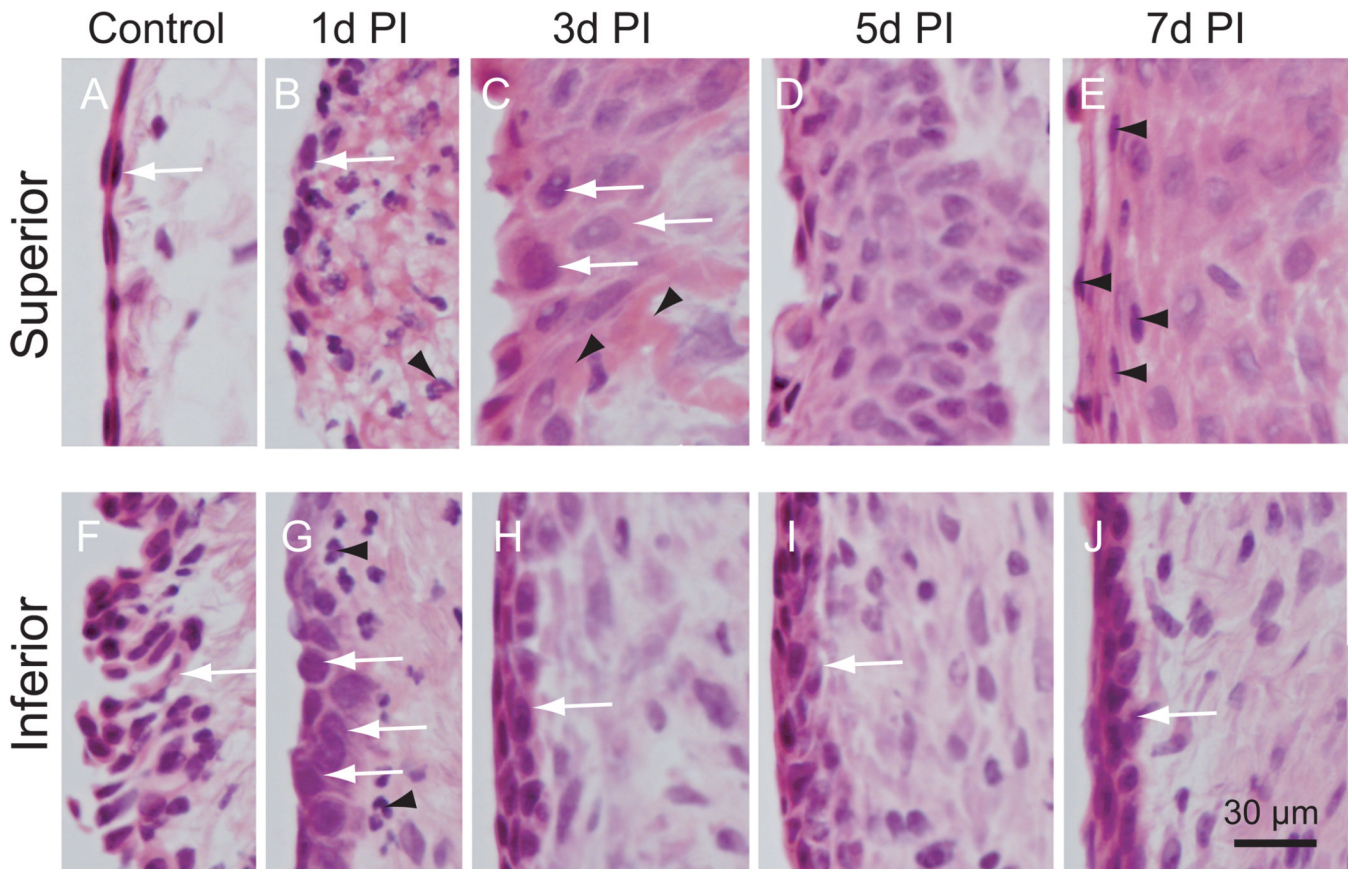

Figure 7.

Cellular changes in the rat vocal fold epithelium following injury. Microscopy images (corresponding to small black boxes in Figure 5 F–J) at high magnification (400×) showing detailed cellular morphology. Superior: upper black boxes in Figure 5; Inferior: lower black boxes in Figure 5. Arrow in A: stratified squamous cells; Arrows in B, G, H, I and J: newly recruited epithelial cells; Arrowheads in B and G: neutrophil-like cells; Arrows in C: large epithelial cells embedded in fibrin matrix; Arrowheads in C: fibrin matrix; Arrowheads in E: newly recruited stratified squamous cells; Arrow in F: ciliated pseudocolumnar formation. PI: post-injury.

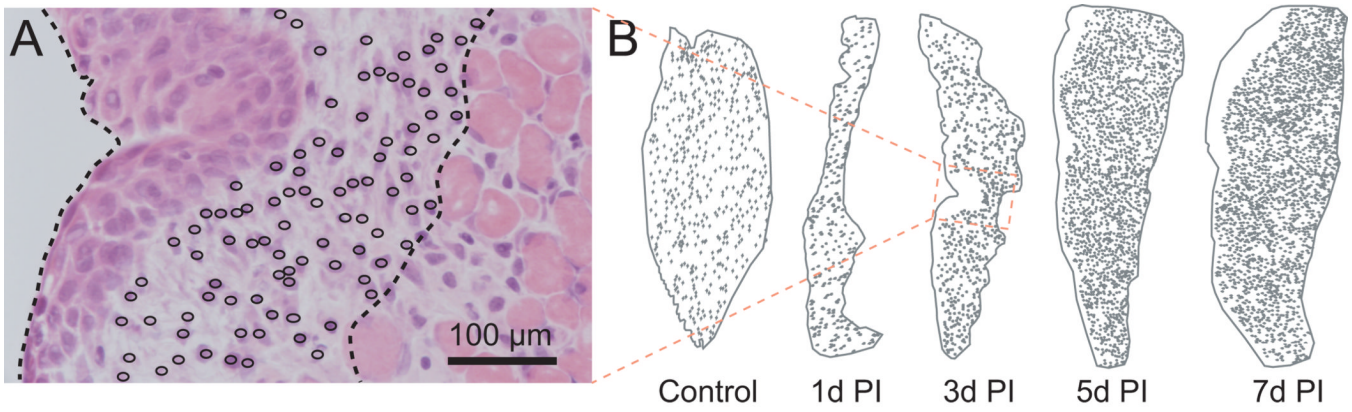

Figure 8.
Representative cellular maps of the vocal fold mucosa following injury, illustrating changes in mucosal cross-sectional area and lamina propria cell density. A: Representative stereological analysis showing a measurement probe superimposed over an H&E stained section of the vocal fold mucosa 3 days post-injury. A dotted contour line shows the boundary of the mucosa, and open circles mark each cell within the lamina propria. B: Representative cellular maps (low magnification) at sequential post-injury time points. PI: post-injury.

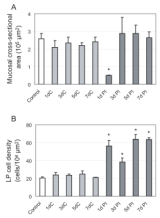

Figure 9.

Quantitative analysis of sequential changes in rat vocal fold mucosa following a unilateral stripping injury. A: Histogram showing significant change in mucosal cross-sectional area post-injury compared to control. B: Histogram showing significant increase in lamina propria cell density post-injury compared to control. White bars (control) reflect mucosa from naïve animals with no injury to either vocal fold; light grey bars reflect non-injured (contralateral) mucosa from experimental animals; dark grey bars reflect injured mucosa from experimental animals.

*: $p < 0.05$; LP: lamina propria; C: contralateral non-injured mucosa; PI: post-injury.